RESEARCH ARTICLE | AUGUST 01 2025

Optical characteristics of passivation layers for ultra-low-loss on-chip devices in the mid-infrared

Daewon Suk ; Kiyoung Ko ; Jingyu Kim; Sang-Hee Ko Park; Duk-Yong Choi ; Hansuek Lee

APL Mater. 13, 081102 (2025)
https://doi.org/10.1063/5.0275180

Optical characteristics of passivation layers for ultra-low-loss on-chip devices in the mid-infrared

Cite as: APL Mater. 13, 081102 (2025); doi: 10.1063/5.0275180
Submitted: 11 April 2025 • Accepted: 15 July 2025 •
Published Online: 1 August 2025

Daewon Suk,[1] Kiyoung Ko,[1] Jingyu Kim,[2] Sang-Hee Ko Park,[2] Duk-Yong Choi,[3,a)] and Hansuek Lee[1,a)]

AFFILIATIONS

[1] Department of Physics, Korea Advanced Institute of Science and Technology, Daejeon 34141, Republic of Korea
[2] Department of Material Science and Engineering, Korea Advanced Institute of Science and Technology, Daejeon 34141, Republic of Korea
[3] Laser Physics Centre, Research School of Physics, Australian National University, Canberra, ACT 2601, Australia

[a)] **Authors to whom correspondence should be addressed:** duk.choi@anu.edu.au and hansuek@kaist.ac.kr

ABSTRACT

On-chip photonics offers substantial potential for miniaturizing mid-infrared (mid-IR) optical systems, advancing molecular science and technology across diverse practical applications. However, strong interaction between mid-IR light and chemical species, while beneficial for molecular detection, can also leave these devices, such as ones made with chalcogenide glass, vulnerable to gradual increases in propagation loss caused by the adsorption and diffusion of airborne chemicals. Dense, nanometer-scale atomic layer deposited (ALD) films are commonly employed as protective barriers against surrounding contaminants, but their effectiveness in preserving initial optical loss performance has not been quantitatively assessed. In this study, we investigate both the protective capabilities of ALD coatings and their influence on mid-IR propagation losses. By depositing Al_2O_3 and TiO_2 films on ultra-low-loss microresonators and monitoring changes in propagation loss over several days, we demonstrate that these ALD films effectively prevent long-term loss degradation. Nonetheless, the coating also introduces initial optical losses through two distinct mechanisms, absorption from precursor-derived impurities within the film and increased surface-adsorbed water due to higher surface hydrophilicity. By analyzing the dependence of additional optical loss on film thickness and two distinct precursor chemistries, we clearly distinguish these mechanisms. Our results provide a comprehensive evaluation of mid-IR passivation materials in terms of both passivation capability and optical loss impact, highlighting the critical importance of careful selection and process optimization of passivation films for further performance improvements in integrated mid-IR photonic devices.

I. INTRODUCTION

The mid-infrared (mid-IR) wavelength, also known as the molecular fingerprint region, is highly valued for its strong interaction with the fundamental vibrational modes of various molecules, making it indispensable for applications such as molecular sensing/spectroscopy,[1,2] biochemical imaging,[3–5] and chemical processing.[6,7] Although these applications have traditionally relied on bulky free-space optics, integrated photonics offers a pathway toward compact and highly versatile chip-scale solutions. Recent advancements in on-chip quantum cascade lasers,[8,9] mid-IR photodetectors,[10,11] and their spectroscopic applications[12–14] have demonstrated the feasibility of these goals. Concurrently, remarkable advancements have been made in reducing propagation loss in mid-IR waveguides by using materials such as Si,[15–17] Ge,[18–20] SiGe,[21–24] and chalcogenide glasses (ChGs).[25–28] One notable milestone is the demonstration of propagation losses of as low as 0.52 dB/m on a ChG platform,[29] on par with that of state-of-the-art mid-IR fibers,[30] paving the way for implementing versatile ultra-high-Q microresonators in this wavelength range.

Despite these advancements, maintaining the ultra-low-loss performance, such as that achieved on the ChG platform, remains challenging, mainly due to the adsorption and infiltration of airborne chemical contaminants through the typically thinner cladding

layers used in on-chip devices compared to those of optical fibers. In particular, the exceptional sensitivity of mid-IR light to chemical species makes these on-chip devices prone to progressive loss increases over time by, for example, water molecules from the surrounding environment. To manage this issue, atomic layer deposition (ALD) has often been employed to thinly coat the devices with dense protective films that suppress the diffusion of contaminants.[31–33] However, to the best of our knowledge, the effectiveness of these films in preserving the initial loss performance of mid-IR devices and how the films themselves affect the propagation loss have not been optically characterized yet because such effects were masked by the relatively high scattering loss on previous on-chip mid-IR devices.

In this work, we investigate both the passivation performance and additional optical losses introduced by ALD films when applied to the ChG-based ultra-low-loss resonator platforms. The results revealed that while the ALD films effectively preserve propagation loss for more than five days in an ambient environment, they also introduce the initial additional loss, attributed to two mechanisms: first, absorption by precursor-derived impurities incorporated into the film, and second, change in surface hydrophilicity that affects the concentration of adsorbed water. These loss mechanisms were discriminated and quantitatively analyzed by measuring, as a function of wavelength, additional losses introduced by ALD Al_2O_3 and TiO_2 films of various thicknesses, each using different precursor chemistries. The findings presented here provide insights for selecting and processing passivation films suitable for developing ultra-low-loss mid-IR photonic circuits on a chip, paving the way for broad practical applications of mid-IR photonics.

II. METHODS

The passivation performance of ALD films and their impact on device propagation loss were analyzed in the mid-IR range using ultra-low-loss resonators made of ChG materials. These resonators, having a unique trapezoidal cross-section geometry [Fig. 1(a)], exhibit the lowest mid-IR propagation loss among on-chip platforms, making them ideal for monitoring even minute changes in the loss by diffusion of contaminants or by the nanometer-thick films themselves. The device in specific consists of an As_2Se_3 core, As_2S_3 top/bottom claddings that minimize absorption loss from the SiO_2 substrate and external contaminants [Fig. 1(b)], and a 10 nm thick Ge-As-Se uppermost layer that prevents the crystallization of the arsenic-based core and cladding materials. The mid-IR loss of these resonators was precisely characterized by measuring their quality factors (Q-factors), which is inversely proportional to the loss, using a free-space measurement setup that includes a calibrated free-space Michelson interferometer (MI, 75.25 MHz) as a frequency reference [Fig. 1 (e)]. The intrinsic Q-factors (Q_{int}) of the resonators over the 3.2–3.9 μm wavelength range were measured to be between

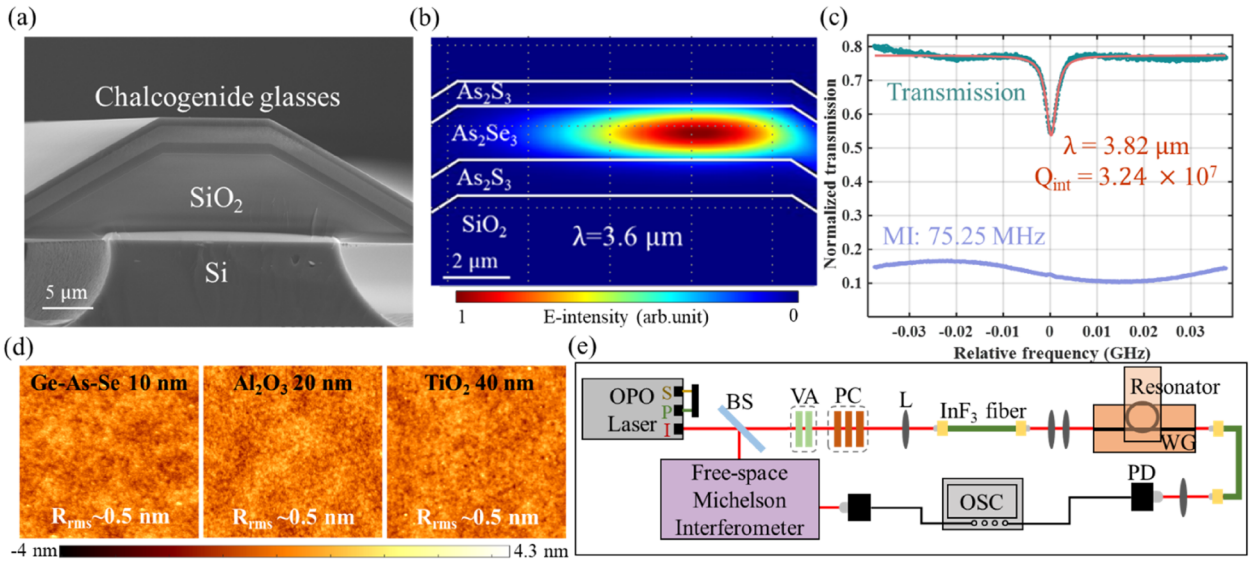

FIG. 1. (a) Scanning electron microscope image of the trapezoidal on-chip resonator cross section. (b) An intensity profile of the optical mode calculated using the measured geometry is presented. The mode is asymmetric, being shifted toward the outer rim of the resonator due to its bent structure. The thickness of each layer (t), radius (R), wedge angle (θ), and top width (w) of the device are as follows: t_{SiO_2} = 8 μm, $t_{As_2S_3\,(bottom)}$ = 1.1 μm, $t_{As_2Se_3\,(core)}$ = 1.7 μm, $t_{As_2S_3\,(top)}$ = 0.8 μm, R = 2.5 mm, θ = 28.9°, w = 10.7 μm. (c) Highest Q-factor measured on the resonator, showing an intrinsic Q-factor (Q_{int}) of 3.24 ×10^7 at a wavelength of 3.82 μm. The turquoise line shows the bus waveguide transmission data; the orange line is the Lorentzian fitting; and the blue line is the Michelson interferometer (MI) signal used as a frequency reference. (d) Surface roughness of resonators with different uppermost material layers, measured by atomic force microscopy. R_{rms} values indicate the root mean square roughness measured over a 2 × 2 μm^2 area. (e) Schematic of the free-space mid-IR measurement setup. A continuously tunable optical parametric oscillation type laser (Aculight Argos 2400 C module, linewidth <1MHz) was used as the pump source. BS: beam splitter, VA: variable attenuator, PC: polarization controller, L: lens, WG: bus waveguide, PD: photodetector, and OSC: oscilloscope.

32 and 5×10^6 [Fig. 1(c)], corresponding to an optical loss of 0.6 to 5 dB/m, depending on the wavelength. More details can be found in Refs. 29, 34, and 35.

Two different passivation materials, Al_2O_3 and TiO_2, were coated onto the surface of these resonators by O_2 plasma-enhanced ALD (PEALD). Different types of precursors were chosen to check the effect of chemical residues originating from them: an organic precursor trimethylaluminum (TMA) for Al_2O_3, and an inorganic $TiCl_4$ for TiO_2. The deposition temperature was set below the glass transition temperature of composing ChGs (187 °C for As_2S_3 and 178 °C for As_2Se_3),[36] being 120 °C for Al_2O_3 and 130 °C for TiO_2. The roughness of the device surface remained nearly identical after the ALD coating as depicted in Fig. 1 (d), meaning that the scattering loss of the devices was not altered by the coating process. In addition, the absence of crystallite states on the TiO_2 ALD films, which are known to form rutile crystal phases under certain conditions,[37] was confirmed by x-ray diffraction.

III. RESULTS AND DISCUSSION

A. Passivation performance of ALD films

Optical characterization of the PEALD coated and uncoated devices revealed that while both the Al_2O_3 and TiO_2 films effectively passivate the resonators, allowing them to maintain their ultra-high-Q performance over time under ambient conditions, a noticeable reduction in the initial device performance occurs by their deposition. The passivation performance of the films was analyzed by monitoring changes in Q_{int} while placing the devices in a temperature- and humidity-controlled environment for five to ten days, without exposing them to external light to prevent photoinduced changes in the ChG materials. As shown in Fig. 2, despite the thick top cladding layer, the resonator without an ALD coating exhibited a noticeable decrease in Q_{int} to approximately half of its original value over ten days, or ~0.3 dB per day, whereas devices incorporating an additional Al_2O_3 or TiO_2 layer maintained their Q_{int} over similar periods. However, the coating process simultaneously decreased the initial Q_{int} of the device from values above 10^7 to approximately 5×10^6 and 3×10^6 for TiO_2 and Al_2O_3 coated resonators, respectively, which is a significantly large change considering their thickness of just a few nanometers.

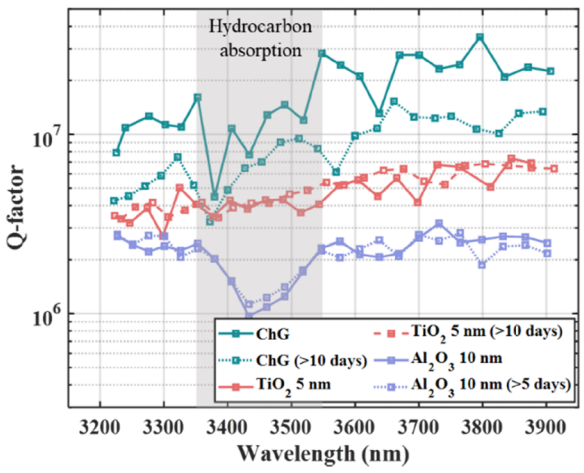

FIG. 2. Q_{int} spectra of uncoated, Al_2O_3 coated, and TiO_2 coated resonators measured right after the deposition of ALD films (or right after its fabrication in the case of the uncoated resonator) and after being placed under ambient conditions for five to ten days. The resonators with an ALD passivation layer show no clear sign of degradation, demonstrating the passivation property of the films.

The modified Q_{int} of Al_2O_3 and TiO_2 coated resonators show different spectral tendencies compared to the uncoated resonators and with each other, as depicted in Fig. 2. According to Ref. 29, the Q_{int} spectra of uncoated resonators in this wavelength range are determined by the absorption loss from hydrocarbons and water, adsorbed to the device surface. The absorption from hydrocarbons (C–H) causes Q_{int} to locally decrease over the 3.35–3.55 μm wavelengths,[26,29] while the absorption from water, having its peak at 2.9 μm and an extremely broad tail, limits the overall Q_{int} value over the measured 3.2–3.9 μm wavelength range.[26,29,36,38] This causes Q_{int} to gradually increase together with the wavelength, since the intensity of water absorption decreases as the wavelength gets farther from its peak. In the case of Al_2O_3-coated resonators, the Q_{int} spectra are nearly flat over the measured wavelengths, except for the hydrocarbon absorption band, which implies that the loss is not limited by the absorption from surface-adsorbed water molecules. In contrast, the overall Q_{int} spectra of TiO_2-coated resonators are mostly similar to that of the uncoated resonators, except that their absolute values are around one-third lower and the hydrocarbon absorption dips are not visible.

To understand these spectral differences and reveal the origin of loss caused by each PEALD film, resonators with various ALD film thicknesses were fabricated and the additional loss caused by them was analyzed as a function of their thickness. This method allows for a clear distinction between whether the additional loss originates from within the ALD film (film material absorption) or from its surface (absorption from surface-adsorbed contaminants), as the intensity of two losses exhibits different proportionality to the film thickness. If absorption from the film material itself is the origin, the additional loss by the film will increase linearly proportional to its thickness. In contrast, if surface-related loss factors are the dominant cause, the additional loss is expected to remain nearly constant since the optical power at the surface is only minimally affected by the addition of films with nanometer-scale thickness.

B. Optical loss by Al_2O_3 passivation films

In the case of PEALD Al_2O_3 films, material absorption loss was identified as the dominant loss factor. Comparing the average Q_{int} spectra of resonators coated with 10 and 20 nm Al_2O_3 films reveals that the Q_{int} values decrease proportionally to the film thickness, as depicted in Fig. 3(a). The additional optical losses induced by the 10 and 20 nm Al_2O_3 films ($\alpha^*_{10nm}, \alpha^*_{20nm}$) were extracted by subtracting the propagation loss of an uncoated resonator (α_{0nm}), converted from measured Q_{int} ($Q_{int} = 2\pi n_g/\lambda\alpha$, n_g: group refractive index, λ: wavelength), from that of Al_2O_3 film-deposited resonators (α_{10nm}, α_{20nm}), as shown in Fig. 3(b). The ratio of these additional losses was close to 2 in regions excluding the hydrocarbon absorption loss area [Fig. 3(b)], indicating that the loss originates from the intrinsic material absorption of the film. This result demonstrates that, despite their nanometer-scale

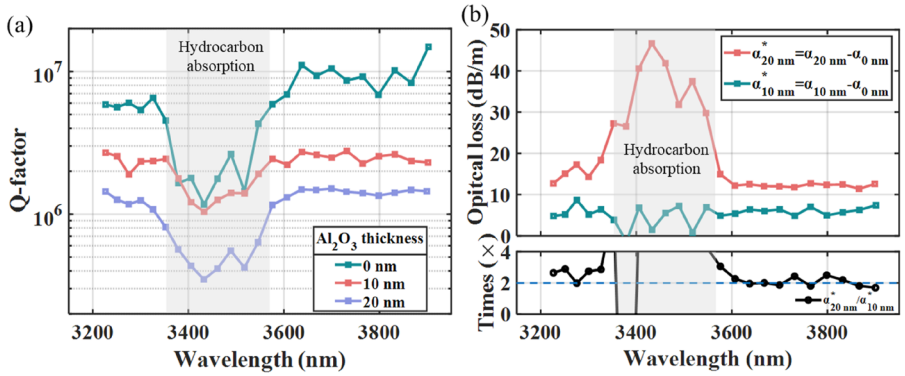

FIG. 3. Mid-IR Q_{int} spectra of resonators coated with Al_2O_3 films. (a) Comparison of Q_{int} spectra for resonators with varying Al_2O_3 layer thicknesses. The overall Q_{int} values monotonically decrease with increasing Al_2O_3 film thickness. (b) Spectra of additional optical loss caused by the Al_2O_3 films. The additional loss was calculated by first converting Q_{int} into propagation loss and then subtracting the loss of resonators with and without the Al_2O_3 film. The black line below indicates the ratio between the additional loss caused by the 10 and 20 nm Al_2O_3 films.

thicknesses, PEALD Al_2O_3 films fabricated using the previously mentioned conditions can significantly contribute to the mid-IR loss of the device.

The material extinction coefficient of the film was roughly estimated from the loss to be $k_{film} \sim 10^{-2}$, which is more than 100 times larger than that of fused silica on the same wavelength range.[39] This significant deviation of the extinction coefficient from pristine Al_2O_3, which is known to be transparent under 4 μm wavelengths,[40] is likely caused by impurities within the PEALD film. The films in this study were deposited at 120 °C to avoid the phase transition of chalcogenide glass materials. However, this temperature is insufficient to effectively remove –OH-related residues originating from the organic precursor TMA and oxygen, which are typically mitigated when deposition occurs above 250 °C.[41,42] As a result, the high –OH content inside the Al_2O_3 films is suspected to cause a strong absorption peak at 2.9 μm wavelength, with a broad tail that produces the flat additional loss spectra over the measured 3.2–3.9 μm range in Fig. 3(b).

C. Optical loss by TiO_2 passivation films

Compared to Al_2O_3, the additional loss by TiO_2 films, deposited using inorganic oxygen plasma and $TiCl_4$ precursors, was found to be originating from its surface by analyzing its thickness dependence. The Q_{int} spectra of TiO_2-deposited resonators [Fig. 4(a)] show that while Q_{int} decrease after film deposition, the extent of the reduction is independent of thickness, as more clearly observed in the additional loss data and the near unity ratio between them [Fig. 4(b)]. This suggests that the material absorption loss of this TiO_2 film, free from OH impurities due to the use of inorganic precursors,[43,44] is negligibly small at this wavelength unlike that of Al_2O_3. Instead, this thickness-independent additional loss can be deduced as originating from the film surface as explained previously.

This additional loss from the surface is speculated to be caused by an increased concentration of surface-adsorbed water due to strong hydrophilicity of the TiO_2 film. Spectral analysis of the resonator Q_{int} and hydrophilicity measurements were conducted to support this hypothesis. In Ref. 29, it was demonstrated that the total loss (α_{tot}) of an on-chip mid-IR resonator can be decomposed into three numerically calculable loss factors,

$$\alpha_{tot} = \alpha_{material} + \alpha_{water} + \alpha_{scatter},$$

where $\alpha_{material}$, α_{water}, and $\alpha_{scatter}$ correspond to absorption loss from its composing materials, loss coming from surface-adsorbed water molecules, and scattering loss due to surface roughness, respectively.

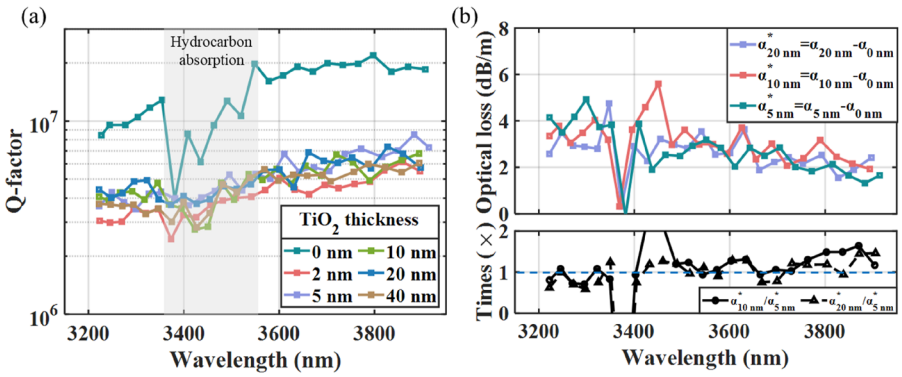

FIG. 4. Mid-IR Q_{int} spectra of resonators coated with TiO_2 films. (a) Q_{int} spectra of resonators with varying TiO_2 layer thicknesses. The decrease in Q_{int} is independent of the thickness. (b) Additional loss by TiO_2 deposition, calculated in the same way as done for Al_2O_3 films. The ratios between the additional losses by 5, 10, and 20 nm TiO_2 films (black line below) are near unity over the whole measured spectrum range.

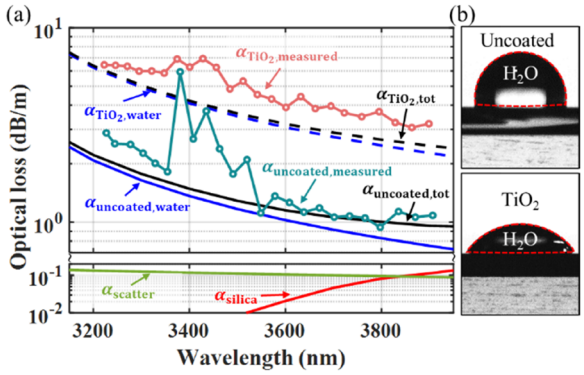

FIG. 5. (a) Numerically expected optical loss of uncoated and TiO_2-coated resonators compared to measured values. The optical loss spectrum of the TiO_2-coated resonator shown here represents the average of all optical loss spectra of TiO_2-coated resonators, converted from Q_{int} in Fig. 4(a). (b) The difference in water contact angle between the uncoated Ge-As-Se ChG resonator surfaces and the TiO_2 film.

Each loss factor exhibits distinct wavelength dependence, as shown in Fig. 5(a), allowing us to determine the dominant loss mechanism. Numerical calculations in Fig. 5(a) show that $\alpha_{material}$, which is reduced to α_{silica} coming from the SiO_2 substrate in this case as all the ChG materials are transparent in the mid-IR, and $\alpha_{scatter}$ are negligibly small, while the spectral envelopes of Q_{int} for both uncoated and coated devices are dominated by α_{water}. In general, α_{water} is proportional to the optical field intensity multiplied by the concentration of adsorbed water at the outermost air-facing surface. Assuming that the water concentration on the TiO_2 surface is three times higher than on the ChG layer ($\alpha_{TiO_2,\ water} = \alpha_{uncoated,\ water} \times 3$), the numerically calculated optical losses for the TiO_2-coated resonators closely match the measured values. To further support the hypothesis of higher water concentration on the TiO_2 surface compared to ChG, their hydrophilicity was compared by measuring the water droplet contact angle, as shown in Fig. 5(b). The TiO_2 surface exhibited a contact angle of 50.4°, significantly lower than the 100.4° angle measured on the uncoated ChG device surface, confirming its higher hydrophilicity.

IV. CONCLUSION

In conclusion, we optically analyzed the effectiveness of Al_2O_3 and TiO_2 PEALD passivation films in preserving the loss performance of on-chip devices at 3–4 μm mid-IR wavelengths by depositing them on ultra-low-loss microresonators on a chip. While these films effectively prevented the degradation of loss by blocking moisture diffusion from the air, the films themselves were found to contribute significantly to mid-IR propagation loss through two distinct mechanisms. Low-temperature PEALD Al_2O_3 films made from an organic precursor TMA exhibited strong material absorption loss in the mid-IR due to the incorporation of OH-related impurities from TMA. In contrast, PEALD TiO_2 films made from an inorganic precursor $TiCl_4$ showed negligible material absorption but increased the optical loss coming from surface-adsorbed water due to their strong hydrophilicity.

The strong material absorption of Al_2O_3 films could be resolved by using an inorganic precursor $AlCl_3$ instead of TMA,[45,46] similar to the case of the TiO_2 film, or by performing the PEALD process at a temperature higher than 250 °C. However, the latter solution can only be applied to devices made with materials that can withstand this temperature, for instance, ChG materials with T_g higher than 250 °C such as Ge-Sb-S.[47,48] The problem of strong hydrophilicity in TiO_2 films could be mitigated by applying treatments that make the surface hydrophobic, such as thinly coating it with fluoropolymers[26] or fluoroalkylsilane self-assembled monolayers.[49] In addition, ALD layers that are natively hydrophobic[50] could be applied as well, although their passivation properties should be tested beforehand.

To the best of our knowledge, this is the first systematic analysis of the impact of ALD layers on the loss performance of mid-IR photonic devices, highlighting the necessity of considering deposition conditions and chemical characteristics of the films when coating them on ultra-low-loss devices. Moreover, the results suggest that chemical post-treatments targeted to reduce the adsorption of specific airborne molecules on the device surfaces can further enhance the loss performance. We anticipate that this study will contribute to the broader exploration of passivation materials for ultra-low-loss mid-IR circuits on a chip, enhancing the overall optical performance of mid-IR photonic devices.

ACKNOWLEDGMENTS

This work was supported by the Samsung Research Funding & Incubation Center of Samsung Electronics under Project No. SRFC-IT1801-03, and the National Research Foundation of Korea (NRF) grant funded by the Korea government (MSIT) (Grant Nos. RS-2024-00408271 and 2023R1A2C2004472). H.L. acknowledges the support from the KAIST Cross-Generation Collaborative Lab project. The authors thank Professor Xunsi Wang and Professor Rongping Wang for providing purified chalcogenide glass ingots for evaporation sources. Work related to PEALD TiO2 used the ACT node of the NCRIS-enabled Australian National Fabrication Facility (ANFF-ACT)

AUTHOR DECLARATIONS

Conflict of Interest

The authors have no conflicts to disclose.

Author Contributions

D.S. and K.K. contributed equally to this work.

Daewon Suk: Conceptualization (equal); Data curation (equal); Formal analysis (equal); Investigation (equal); Methodology (equal); Visualization (equal); Writing – original draft (equal); Writing – review & editing (equal). **Kiyoung Ko**: Conceptualization (equal); Data curation (equal); Formal analysis (equal); Investigation (equal); Methodology (equal); Visualization (equal); Writing – original draft (equal); Writing – review & editing (equal). **Jingyu Kim**: Investigation (equal); Writing – original draft (equal); Writing – review & editing (equal). **Sang-Hee Ko Park**: Methodology (equal);

Writing – original draft (equal); Writing – review & editing (equal). **Duk-Yong Choi**: Conceptualization (equal); Formal analysis (equal); Funding acquisition (equal); Methodology (equal); Project administration (equal); Supervision (equal); Writing – original draft (equal); Writing – review & editing (equal). **Hansuek Lee**: Conceptualization (equal); Formal analysis (equal); Funding acquisition (equal); Methodology (equal); Project administration (equal); Supervision (equal); Writing – original draft (equal); Writing – review & editing (equal).

DATA AVAILABILITY

The data that support the findings of this study are available from the corresponding author upon reasonable request.

REFERENCES

[1] B. Spaun, P. B. Changala, D. Patterson, B. J. Bjork, O. H. Heckl, J. M. Doyle, and J. Ye, "Continuous probing of cold complex molecules with infrared frequency comb spectroscopy," Nature **533**(7604), 517–520 (2016).

[2] M. A. Abbas, Q. Pan, J. Mandon, S. M. Cristescu, F. J. M. Harren, and A. Khodabakhsh, "Time-resolved mid-infrared dual-comb spectroscopy," Sci. Rep. **9**(1), 17247 (2019).

[3] D. Zhang, C. Li, C. Zhang, M. N. Slipchenko, G. Eakins, and J.-X. Cheng, "Depth-resolved mid-infrared photothermal imaging of living cells and organisms with submicrometer spatial resolution," Sci. Adv. **2**(9), e1600521 (2016).

[4] M. Tamamitsu, K. Toda, H. Shimada, T. Honda, M. Takarada, K. Okabe, Y. Nagashima, R. Horisaki, and T. Ideguchi, "Label-free biochemical quantitative phase imaging with mid-infrared photothermal effect," Optica **7**(4), 359–366 (2020).

[5] L. Shi, X. Liu, L. Shi, H. T. Stinson, J. Rowlette, L. J. Kahl, C. R. Evans, C. Zheng, L. E. P. Dietrich, and W. Min, "Mid-infrared metabolic imaging with vibrational probes," Nat. Methods **17**(8), 844–851 (2020).

[6] F. J. Garcia-Vidal, C. Ciuti, and T. W. Ebbesen, "Manipulating matter by strong coupling to vacuum fields," Science **373**(6551), eabd0336 (2021).

[7] A. Thomas, L. Lethuillier-Karl, K. Nagarajan, R. M. A. Vergauwe, J. George, T. Chervy, A. Shalabney, E. Devaux, C. Genet, J. Moran, and T. W. Ebbesen, "Tilting a ground-state reactivity landscape by vibrational strong coupling," Science **363**(6427), 615–619 (2019).

[8] B. Meng, M. Singleton, J. Hillbrand, M. Franckié, M. Beck, and J. Faist, "Dissipative Kerr solitons in semiconductor ring lasers," Nat. Photonics **16**(2), 142–147 (2022).

[9] N. Opačak, D. Kazakov, L. L. Columbo, M. Beiser, T. P. Letsou, F. Pilat, M. Brambilla, F. Prati, M. Piccardo, F. Capasso, and B. Schwarz, "Nozaki–Bekki solitons in semiconductor lasers," Nature **625**(7996), 685–690 (2024).

[10] J. Hillbrand, L. Matthieu Krüger, S. Dal Cin, H. Knötig, J. Heidrich, A. Maxwell Andrews, G. Strasser, U. Keller, and B. Schwarz, "High-speed quantum cascade detector characterized with a mid-infrared femtosecond oscillator," Opt. Express **29**(4), 5774 (2021).

[11] B. Hinkov, F. Pilat, L. Lux, P. L. Souza, M. David, A. Schwaighofer, D. Ristanić, B. Schwarz, H. Detz, A. M. Andrews, B. Lendl, and G. Strasser, "A mid-infrared lab-on-a-chip for dynamic reaction monitoring," Nat. Commun. **13**(1), 4753 (2022).

[12] S. C. Lee, S. Park, D. Suk, J. Hwang, K. Ko, W. B. Cho, D.-Y. Choi, K.-H. Ko, F. Rotermund, and H. Lee, "On-chip mid-infrared dispersive wave generation at targeted molecular absorption wavelengths," APL Photonics **9**(8), 080802 (2024).

[13] D. Grassani, E. Tagkoudi, H. Guo, C. Herkommer, F. Yang, T. J. Kippenberg, and C.-S. Brès, "Mid infrared gas spectroscopy using efficient fiber laser driven photonic chip-based supercontinuum," Nat. Commun. **10**(1), 1553 (2019).

[14] A. Y. Hwang, H. S. Stokowski, T. Park, M. Jankowski, T. P. McKenna, C. Langrock, J. Mishra, V. Ansari, M. M. Fejer, and A. H. Safavi-Naeini, "Mid-infrared spectroscopy with a broadly tunable thin-film lithium niobate optical parametric oscillator," Optica **10**(11), 1535–1542 (2023).

[15] S. A. Miller, M. Yu, X. Ji, A. G. Griffith, J. Cardenas, A. L. Gaeta, and M. Lipson, "Low-loss silicon platform for broadband mid-infrared photonics," Optica **4**(7), 707 (2017).

[16] A. Spott, Y. Liu, T. Baehr-Jones, R. Ilic, and M. Hochberg, "Silicon waveguides and ring resonators at 5.5 μm," Appl. Phys. Lett. **97**(21), 213501 (2010).

[17] J. S. Penades, A. Ortega-Moñux, M. Nedeljkovic, J. G. Wangüemert-Pérez, R. Halir, A. Z. Khokhar, C. Alonso-Ramos, Z. Qu, I. Molina-Fernández, P. Cheben, and G. Z. Mashanovich, "Suspended silicon mid-infrared waveguide devices with subwavelength grating metamaterial cladding," Opt. Express **24**(20), 22908 (2016).

[18] D. Ren, C. Dong, S. J. Addamane, and D. Burghoff, "High-quality microresonators in the longwave infrared based on native germanium," Nat. Commun. **13**(1), 5727 (2022).

[19] D. Ren, C. Dong, J. Høvik, M. I. Khan, A. Aksnes, B.-O. Fimland, and D. Burghoff, "Low-loss hybrid germanium-on-zinc selenide waveguides in the longwave infrared," Nanophotonics **13**(10), 1815–1822 (2024).

[20] G. Z. Mashanovich, C. J. Mitchell, J. S. Penades, A. Z. Khokhar, C. G. Littlejohns, W. Cao, Z. Qu, S. Stanković, F. Y. Gardes, T. B. Masaud, H. M. H. Chong, V. Mittal, G. S. Murugan, J. S. Wilkinson, A. C. Peacock, and M. Nedeljkovic, "Germanium mid-infrared photonic devices," J. Lightwave Technol. **35**(4), 624–630 (2017).

[21] R. Armand, M. Perestjuk, A. Della Torre, M. Sinobad, A. Mitchell, A. Boes, J.-M. Hartmann, J.-M. Fedeli, V. Reboud, P. Brianceau, A. De Rossi, S. Combrié, C. Monat, and C. Grillet, "Mid-infrared integrated silicon–germanium ring resonator with high Q-factor," APL Photonics **8**(7), 071301 (2023).

[22] N. Koompai, T. H. N. Nguyen, V. Turpaud, J. Frigerio, V. Falcone, S. Calcaterra, L. Lucia, A. Bousseksou, R. Colombelli, J.-R. Coudevylle, D. Bouville, C. Alonso-Ramos, L. Vivien, G. Isella, and D. Marris-Morini, "Long-wave infrared integrated resonators in the 7.5–9 μm wavelength range," Appl. Phys. Lett. **123**(3), 031109 (2023).

[23] M. Montesinos-Ballester, V. Vakarin, Q. Liu, X. Le Roux, J. Frigerio, A. Ballabio, A. Barzaghi, C. Alonso-Ramos, L. Vivien, G. Isella, and D. Marris-Morini, "Ge-rich graded SiGe waveguides and interferometers from 5 to 11 μm wavelength range," Opt. Express **28**(9), 12771–12779 (2020).

[24] V. Turpaud, T.-H.-N. Nguyen, H. Dely, N. Koompai, A. Bricout, J.-M. Hartmann, N. Bernier, J. Krawczyk, G. Lima, S. Edmond, E. Herth, C. Alonso-Ramos, L. Vivien, and D. Marris-Morini, "Low-loss SiGe waveguides for mid-infrared photonics fabricated on 200 mm wafers," Opt. Express **32**(10), 17400 (2024).

[25] H. Lin, Y. Xiang, L. Li, K. McLaughlin, Y. Liu, Y. Chillakuru, E. Koontz, J. D. Musgraves, K. Richardson, and C. Ni, "High-Q mid-infrared chalcogenide glass resonators for chemical sensing," in *2014 IEEE Photonics Society Summer Topical Meeting Series* (IEEE, 2014), pp. 61–62.

[26] P. Ma, D.-Y. Choi, Y. Yu, X. Gai, Z. Yang, S. Debbarma, S. Madden, and B. Luther-Davies, "Low-loss chalcogenide waveguides for chemical sensing in the mid-infrared," Opt. Express **21**(24), 29927–29937 (2013).

[27] X. Xia, Q. Chen, C. Tsay, C. B. Arnold, and C. K. Madsen, "Low-loss chalcogenide waveguides on lithium niobate for the mid-infrared," Opt. Lett. **35**(19), 3228–3230 (2010).

[28] H. Lin, L. Li, Y. Zou, S. Danto, J. D. Musgraves, K. Richardson, S. Kozacik, M. Murakowski, D. Prather, P. T. Lin, V. Singh, A. Agarwal, L. C. Kimerling, and J. Hu, "Demonstration of high-Q mid-infrared chalcogenide glass-on-silicon resonators," Opt. Lett. **38**(9), 1470–1472 (2013).

[29] K. Ko, D. Suk, D. Kim, S. Park, B. Sen, D.-G. Kim, Y. Wang, S. Dai, X. Wang, R. Wang, B. J. Chun, K.-H. Ko, P. T. Rakich, D.-Y. Choi, and H. Lee, "A mid-infrared Brillouin laser using ultra-high-Q on-chip resonators," Nat. Commun. **16**(1), 2707 (2025).

[30] J. Wang, G. Wu, Z. Feng, J. Wang, Y. Wang, K. Jiao, X. Wang, S. Bai, P. Zhang, Z. Zhao, R. Wang, X. Wang, and Q. Nie, "Se-H-free As_2Se_3 fiber and its spectral applications in the mid-infrared," Opt. Express **30**(13), 24072–24083 (2022).

[31] A. I. Abdulagatov, Y. Yan, J. R. Cooper, Y. Zhang, Z. M. Gibbs, A. S. Cavanagh, R. G. Yang, Y. C. Lee, and S. M. George, "Al_2O_3 and TiO_2 atomic layer deposition on copper for water corrosion resistance," ACS Appl. Mater. Interfaces **3**(12), 4593–4601 (2011).

[32] M. D. Groner, S. M. George, R. S. McLean, and P. F. Carcia, "Gas diffusion barriers on polymers using Al_2O_3 atomic layer deposition," Appl. Phys. Lett. **88**(5), 051907 (2006).

[33]E. Langereis, M. Creatore, S. B. S. Heil, M. C. M. van de Sanden, and W. M. M. Kessels, "Plasma-assisted atomic layer deposition of Al_2O_3 moisture permeation barriers on polymers," Appl. Phys. Lett. **89**(8), 081915 (2006).
[34]D.-G. Kim, S. Han, J. Hwang, I. H. Do, D. Jeong, J.-H. Lim, Y.-H. Lee, M. Choi, Y.-H. Lee, D.-Y. Choi, and H. Lee, "Universal light-guiding geometry for on-chip resonators having extremely high Q-factor," Nat. Commun. **11**(1), 5933 (2020).
[35]D. Kim, S. Han, D.-G. Kim, K. Ko, D.-Y. Choi, and H. Lee, "Two-point coupling method to independently control coupling efficiency at different wavelengths," Opt. Lett. **47**(1), 106–109 (2022).
[36]J.-L. Adam and X. Zhang, *Chalcogenide Glasses: Preparation, Properties and Applications* (Woodhead publishing, 2014).
[37]L. Aarik, T. Arroval, R. Rammula, H. Mändar, V. Sammelselg, and J. Aarik, "Atomic layer deposition of TiO_2 from $TiCl_4$ and O_3," Thin Solid Films **542**, 100–107 (2013).
[38]C. Lecaplain, C. Javerzac-Galy, M. L. Gorodetsky, and T. J. Kippenberg, "Mid-infrared ultra-high-Q resonators based on fluoride crystalline materials," Nat. Commun. **7**(1), 13383 (2016).
[39]R. Kitamura, L. Pilon, and M. Jonasz, "Optical constants of silica glass from extreme ultraviolet to far infrared at near room temperature," Appl. Opt. **46**(33), 8118–8133 (2007).
[40]M. E. Innocenzi, R. T. Swimm, M. Bass, R. H. French, A. B. Villaverde, and M. R. Kokta, "Room-temperature optical absorption in undoped α-Al_2O_3," J. Appl. Phys. **67**(12), 7542–7546 (1990).
[41]V. Verlaan, L. R. J. G. van den Elzen, G. Dingemans, M. C. M. van de Sanden, and W. M. M. Kessels, "Composition and bonding structure of plasma-assisted ALD Al_2O_3 films," Physica Status Solidi C **7**(3–4), 976–979 (2010).
[42]E. Langereis, J. Keijmel, M. C. M. Van De Sanden, and W. M. M. Kessels, "Surface chemistry of plasma-assisted atomic layer deposition of Al_2O_3 studied by infrared spectroscopy," Appl. Phys. Lett. **92**(23), 231904 (2008).
[43]N. G. Kubala, P. C. Rowlette, and C. A. Wolden, "Plasma-enhanced atomic layer deposition of anatase TiO_2 using $TiCl_4$," J. Phys. Chem. C **113**(37), 16307–16310 (2009).
[44]J. B. Kinney and R. H. Staley, "Reactions of titanium tetrachloride and trimethylaluminum at silica surfaces studied by using infrared photoacoustic spectroscopy," J. Phys. Chem. **87**(19), 3735–3740 (1983).
[45]L. Aarik, T. Arroval, R. Rammula, H. Mändar, V. Sammelselg, B. Hudec, K. Hušeková, K. Fröhlich, and J. Aarik, "Atomic layer deposition of high-quality Al_2O_3 and Al-doped TiO_2 thin films from hydrogen-free precursors," Thin Solid Films **565**, 19–24 (2014).
[46]A. Heyman and C. B. Musgrave, "A quantum chemical study of the atomic layer deposition of Al_2O_3 using $AlCl_3$ and H_2O as precursors," J. Phys. Chem. B **108**(18), 5718–5725 (2004).
[47]B. Zhang, D. Xia, X. Zhao, L. Wan, and Z. Li, "Hybrid-integrated chalcogenide photonics," Light: Adv. Manuf. **4**(4), 24 (2023).
[48]Y. Hu, K. Tian, T. Li, M. Zhang, H. Ren, S. Qi, A. Yang, X. Feng, and Z. Yang, "Mid-infrared nonlinear optical performances of Ge-Sb-S chalcogenide glasses," Opt. Mater. Express **11**(3), 695–706 (2021).
[49]Y. Wu, H. Sugimura, Y. Inoue, and O. Takai, "Preparation of hard and ultra water-repellent silicon oxide films by microwave plasma-enhanced CVD at low substrate temperatures," Thin Solid Films **435**(1–2), 161–164 (2003).
[50]I.-K. Oh, K. Kim, Z. Lee, K. Y. Ko, C.-W. Lee, S. J. Lee, J. M. Myung, C. Lansalot-Matras, W. Noh, C. Dussarrat, H. Kim, and H.-B.-R. Lee, "Hydrophobicity of rare earth oxides grown by atomic layer deposition," Chem. Mater. **27**(1), 148–156 (2015).